International Journal of Robotics and Control Systems
Vol. 4, No. 3, 2024, pp. 1059-1074
ISSN 2775-2658
http://pubs2.ascee.org/index.php/ijrcs

Design of Novel STASOSM Controller for FOC Control of Dual Star Induction Motor Drives

Ngoc Thuy Pham [a,1,*]

[a] Department of Electrical Engineering Technology, Industrial University of Ho Chi Minh City, Vietnam
[1] Ngocpham1020@gmail.com
* Corresponding Author

ARTICLE INFO

Article history
Received May 16, 2024
Revised June 24, 2024
Accepted June 27, 2024

Keywords
Backstepping;
Sliding Mode;
Super Twisting;
Six Phase Induction Motor Drives;
FOC

ABSTRACT

In this paper, a Novel Super-Twisting Algorithm combined with Improved Second - Order Sliding Mode (NSTASOSM) for the Field-Oriented Control (FOC) of high performance SPIM drives is proposed. This structure, on the one hand, effectively solves the weaknesses of traditional backstepping control (BS) and sliding mode (SM) control that are the dependent on the change of parameters, load disturbance and the phenomenon of chattering, on the other hand, increases the convergence speed and the reference tracking ability, enhance the robust and stably of drive systems even when working in conditions of uncertain parameter and load disturbances, eliminates the chattering phenomenon. The obtained results by simulation using the Matlab/ Simulink tool verified the performance of this proposed control structure.

1. Introduction

The six-phase induction motor (SPIM) drive system is one of the multiphase alternating current (AC) motor drives that has received much attention. SPIM has been focused on research and development in recent decades and applied in the high-power industrial applications and the systems that require high quality control, reliability and capability high fault tolerance. Especially, in drive systems applied for transportation field such as electric vehicles, aeronautics, ship. Due to its outstanding advantages, it is also gradually replacing three-phase induction motors (IM) in traditional three-phase AC drives in small power applications that require high reliability, accuracy, safety and fault tolerance [1]-[5].

Nowadays, control methods have been developed based on modern vector control strategies AC motor and SPIM drives. Direct Torque Control (DTC) is a simple control strategy which allows controlling two components the flux and torque. DTC has advantages such as the fast response and less dependence on motor parameters, it also is quite simple, does not require any transformation of coordinates or current regulator loops [5]. However, DTC faces major disadvantages such as flux and torque ripples, high switching frequency, noise and mechanical vibration of the motor, low control performance at low speeds [6]-[10]. In opposition to DTC, the Field Oriented Control (FOC), was invented in the 1972 [11], gives fast torque response, a wide speed control range and high efficiency over a wide load variation range, that get by decoupling the torque and the flux control. These problem such as flux and torque ripples, noise and mechanical vibration of the motor, low control performance at low speeds are not appear in this control. Besides the outstanding advantages mentioned above, the

disadvantages of FOC are high sensitivity to the parametric variations of the machine and a great complexity caused by the presence of coordinate transformations and the use of several control variables [12]-[13], so when applying the PID control method for traditional FOC with fixed coefficients, it does not meet the quality of control for high-performance drives [14]. Nonlinear controllers and intelligent controls are proposed [15]-[42] such as Sliding Model (SM), Backstepping control (BS), fuzzy logic and neural network, predictive control, etc. Many studies show that it was difficult to obtain satisfactory control performance when using only an independently control method, especially in the cases applied to control the nonlinear systems. Therefore, to solve this problem, besides continuing to improve control strategy, another approach has paid more and more attention to the hybrid control strategy which combines different control methods [43]-[49].

In [46], a strategy has been proposed, a new hybrid structure combining BS and SM is developed to meet the design principles of FOC control for SPIM drive systems. The SM control strategy is fully consistent with the criteria of a current loop controller that requires fast dynamic response, tracking the reference trajectory with high accuracy, and robustness against external disturbances and variation parameters. However, this SM has the disadvantage of chattering. To overcome this drawback, many methods have been proposed as using exponential and sigmoid functions to reduce chattering, but it also significantly reduces the stability and convergence speed of the system. One other solution uses Integral SM (INTSM) to contribute to reducing steady state errors, increasing response time and being robust to external disturbances. Using integration of state variables into the sliding mode surface leads to large overshoots, which affects the quality of the controller because it creates integral saturation of the integral sliding mode surface, besides, the chattering phenomenon is not much improved in this proposal Other typical proposals such as Higher Order Sliding Mode (HOSM), Second Order Sliding Mode (SOSM), Super-Twisting Algorithm (STA) also have been developed recently. When comparing the application of two types of SOSM control and STA, it shows that STA has a faster response time than SOSM, however, the chattering phenomenon that appears in STA is significantly higher than that of SOSM. This shows that STA has a faster convergence and reference tracking speed, while SOSM allows to significantly reduce chattering and work more robust [50].

In this paper, it is proposed to improve the BS_SM hybrid controller in [46], this proposal combines the super twist algorithm (STA) and improved second-order sliding control for current loop of FOC control SPIM drive, providing an effective tool to eliminate chattering phenomenon while still retaining the main advantages of the STA method and Traditional SM. Additionally, to improve the quality of flux identification, a flux identifier using SM is also used to increase the accuracy and stability of the system. New points in this study:

- The novel hybrid strategy combining the super twisting algorithm and the improved second order sliding mode control (NSTASOSM) give an effective tool for controlling uncertain nonlinear systems because it overcomes the main disadvantages of traditional SM control, which are large control effort and chattering. The advantage of this hybrid current controller is that it can compensate for disturbances, increase convergence speed and the reference tracking ability more quickly and accurately while maintaining continuous control instead of the high-frequency switching. SPIM drive works robust and stably even when working in conditions of uncertain parameter systems and load disturbances. The chattering phenomenon is almost eliminated.
- The BS_ NSTASOSM hybrid controller structure proposed to be developed for SPIM is suitable and meets the requirements of each control loop in SPIM's FOC vector control, helping to improve control quality and performance as well as durability. stability of the SPIM drive system.

The remainder of the paper is presented as follows. Section 2 presents the mathematical model of the SPIM drive, the proposed controller design is presented in detail in Section 3. Simulation results are presented in Section 4. Section 5 concludes.

2. Model of Spim Drive

The drive system under study consists of an SPIM fed by a six-phase Voltage Source Inverter (VSI) and a DC link. A detailed scheme of the drive is provided in Fig. 1 problem formulation.

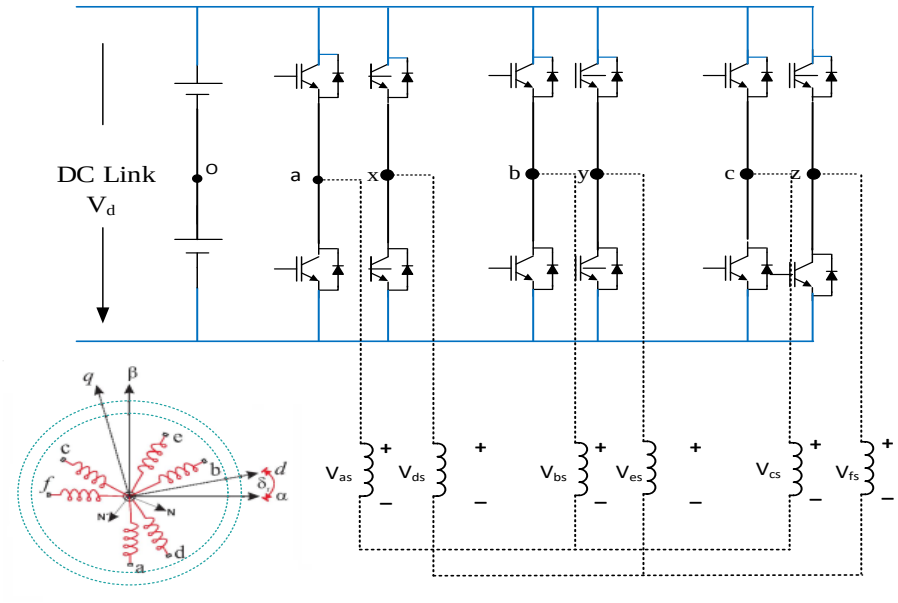

Fig. 1. A SPIM drive general diagram

By applying the Vector Space Decomposition (VSD) technique, the original six-dimensional space of the machine is transformed into three two-dimensional orthogonal subspaces in the stationary reference frame (D-Q), (x - y) and (zl -z2). The voltage space vectors and switching states in the (D-Q) and (x-y) subspaces for a SPVSI was presented in Fig. 2.

This transformation is obtained by means of 6x6 transformation matrix (Eq. (1). In order to develop SPIM model for control purposes, some basic assumptions should be made. Hence, the windings are assumed to be sinusoidally distributed, the magnetic saturation, the mutual leakage inductances, and the core losses are neglected.

$$T_6 = \frac{1}{3}\begin{bmatrix} 1 & \frac{\sqrt{3}}{2} & -\frac{1}{2} & -\frac{\sqrt{3}}{2} & -\frac{1}{2} & 0 \\ 0 & \frac{1}{2} & \frac{\sqrt{3}}{2} & \frac{1}{2} & -\frac{\sqrt{3}}{2} & -1 \\ 1 & -\frac{\sqrt{3}}{2} & -\frac{1}{2} & \frac{\sqrt{3}}{2} & -\frac{1}{2} & 0 \\ 0 & \frac{1}{2} & -\frac{\sqrt{3}}{2} & \frac{1}{2} & \frac{\sqrt{3}}{2} & -1 \\ 1 & 0 & 1 & 0 & 1 & 0 \\ 0 & 1 & 0 & 1 & 0 & 1 \end{bmatrix} \quad (1)$$

The electrical matrix equations in the stationary reference frame for the stator and the rotor may be written as

$$[V_s] = [R_s][I_s] + p([L_s][I_s] + [L_m][I_r])\ 0 = [R_r][I_r] + p([L_r][I_r] + [L_m][I_s]) \quad (2)$$

where: *[V], [I], [R], [L]* and *[Lm]* are voltage, current, resistant, self and mutual inductance vectors, respectively. p is differential operator. Subscript r and s related to the rotor and stator resistance respectively. Since the rotor is squirrel cage, [*V*] is equal to zero. The electromechanical energy conversion only takes place in the only takes place in the *D-Q* subspace and the other subspaces just produce losses. Therefore, the control is based on determining the applied voltage in the *DQ* reference frame. With this transformation, the 6PIM control technique is like the classical three phase IM FOC. The control for the motor in the stationary reference frame is difficult, even for a three phase IM, so the transformation of SPIM model in a dq rotating reference frame to obtain currents with dc components [23] của 1 is necessary, a transformation matrix must be used to represent the stationary reference fame (DQ) in the dynamic reference (d - q). This matrix is given:

$$T_{dq} = \begin{bmatrix} cos(\delta) & -sin(\delta) \\ sin(\delta) & cos(\delta) \end{bmatrix} \tag{3}$$

where δ is the rotor angular position referred to the stator that shows in Fig. 1.

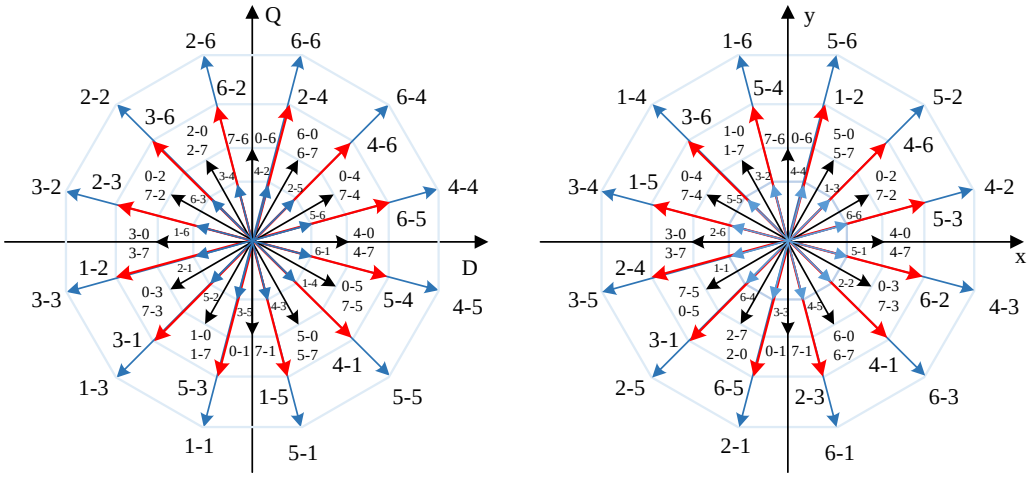

Fig. 2. Voltage space vectors and switching states in the (D-Q) and (x-y) subspaces for a SPVSI

The FOC is the most used strategy in the industrial field. In this control method, the rotor flux is controlled by isd stator current component and the torque by isq quadratic component. We have: $\psi_{rq} = 0; \psi_{rd} = \psi_{rd}$. The model motor dynamics is described by the following space vector differential equations:

$$\begin{cases} \dfrac{d\omega_r}{dt} = \dfrac{3}{2} P \dfrac{\delta\sigma L_s}{J} (\psi_{rd} i_{sq}) - \dfrac{T_L}{J} - B'_{\omega_r} \\ \dfrac{d\psi_{rd}}{dt} = \dfrac{L_m}{\tau_r} i_{sd} - \dfrac{1}{\tau_r} \psi_{rd} \\ L_s \dfrac{di_{sq}}{dt} = -a i_{sq} + L_s \omega_e i_{sd} + b_r \omega_e \psi_{rd} + c u_{sq} \\ L_s \dfrac{di_{sd}}{dt} = -a i_{sd} + L_s \omega_e i_{sq} + b R_r \psi_{rd} + c u_{sd} \end{cases} \tag{4}$$

where: $\sigma = 1 - \frac{L_m^2}{L_s L_r}; \delta = \frac{L_m}{\sigma L_s L_r}; a = \frac{L_m^2 R_r + L_r^2 R_s}{\sigma L_r^2}; b = \frac{L_m^2 R_r}{\sigma L_r^2}; c = \frac{1}{\sigma}; \tau_r = \frac{L_r}{R_r}; B' = \frac{B}{J} u_{sd}, u_{sq}$; i_{sd}, i_{sq} : The components of stator voltage and stator current, respectively; ψ_{rd}, ψ_{rq} : Rotor flux omponents; T_e, T_L : Electromagnetic and load torque; *d-q*; *D-Q*: Synchronous and stationary axis reference frame quantities, respectively; ω_r: the angular velocity (mechanical speed), $\omega_r = (2/P)\omega_{re}$; $\omega_{re,} \omega_{sl,} \omega_e$: the electrical speed respectively Rotor and slip angular and synchronous angular velocity; L_s, L_r: Stator and rotor inductances; L_m: Mutual inductance ; R_s, R_r: Stator and rotor resistances; J: the inertia of motor and load; σ : Total linkage coefficient; P: Number of pole pairs; B: Friction coefficient; τ_r : Rotor and stator time constant. The electromagnetic torque and the slip frequency can be expressed in dq reference frame:

$$T_e = \frac{3P}{2} \frac{L_m}{L_r} \psi_{rd} i_{sq} \tag{5}$$

$$\omega_{sl} = \frac{M}{L_r} \psi_{rd} i_{sq} \tag{6}$$

3. BS_NSTASOSM Control Structure for FOC Control of SPIM Drives

3.1. BS Design for the Outer Speed and Flux Loops

This improve BS controller is designed as that presented in [20], in that, to reduce the influence from the change of parameters and the load disturbance a tracking error integration to be added when designing the BS rotor flux and speed controller and the updated rotor resistance to supply for this controller. The performance and stability of the subsystems is ensured by Lyapunov [2]. Therefore, at each step of the design, a virtual command is created to ensure the convergence of subsystems. The rotor flux and speed tracking errors are defined:

$$\begin{aligned} \varepsilon_\omega &= (\omega_r^* - \omega_r) + k_\omega^{'} \int_0^t (\omega_r^* - \omega_r) dt \\ \varepsilon_\psi &= (\psi_{rd}^* - \psi_{rd}) + k_\psi^{'} \int_0^t (\psi_{rd}^* - \psi_{rd}) dt \end{aligned} \tag{7}$$

The error dynamical equations:

$$\begin{aligned} \dot{\varepsilon}_\omega &= \dot{\omega}_r^* - \frac{3}{2} P \frac{\delta \sigma L_s}{J} \psi_{rd} i_{sq} + \frac{T_l}{J} + B\omega_r + k_\omega^{'}(\omega_r^* - \omega_r) \\ \dot{\varepsilon}_\psi &= \dot{\psi}_{rd}^* + \frac{L_m}{\tau_r} i_{sd} + \frac{1}{\tau_r} \psi_{rd} + k_\psi^{'}(\psi_{rd}^* - \psi_{rd}) \end{aligned} \tag{8}$$

Lyapunov function is chosen:

$$V_{(\omega,\psi)} = \frac{1}{2}\left(\varepsilon_\omega^2 + \varepsilon_\psi^2\right) \tag{9}$$

Differentiating V:

$$\begin{aligned} \frac{dV_{(\omega,\psi)}}{dt} = \varepsilon_\omega \frac{d\varepsilon_\omega}{dt} + \varepsilon_\psi \frac{d\varepsilon_\psi}{dt} &= \varepsilon_\omega \left[\frac{d\omega_r^*}{dt} - k_t \psi_{rd} i_{sq}^* + \frac{T_l}{J} + B\omega_r + k_\omega^{'}(\omega_r^* - \omega_r)\right] \\ &+ \varepsilon_\psi \left[\frac{d\psi_{rd}^*}{dt} + \frac{L_m}{\tau_r} i_{sd}^* + \frac{1}{\tau_r}\psi_{rd} + k_\psi^{'}(\psi_{rd}^* - \psi_{rd})\right] \end{aligned} \tag{10}$$

where: $k_t = \frac{3}{4} P \frac{\delta \sigma L_S}{J}$, k_ω, k_Ψ are positive design constants that determine the closed-loop dynamics. To $V' < 0$, the stabilizing virtual controls are chosen as

$$\begin{aligned} i_{sq}^* &= \frac{1}{k_t \psi_{rd}} \left[k_\omega \varepsilon_\omega + \frac{d\omega_r^*}{dt} + \frac{T_l}{J} + B\omega_r + k_\omega^{'}(\omega_r^* - \omega_r)\right] \\ i_{sd}^* &= \frac{\tau_r}{L_m} \left[k_\psi \varepsilon_\psi + \frac{d\psi_{rd}^*}{dt} + \frac{1}{\tau_r}\psi_{rd} + k_\psi^{'}(\psi_{rd}^* - \psi_{rd})\right] \end{aligned} \tag{11}$$

We obtain:

$$\frac{dV_{(\omega,\psi)}}{dt} = -k_\omega \varepsilon_\omega^2 - k_\psi \varepsilon_\psi^2 < 0 \tag{12}$$

i_{sd} and i_{sq} virtual control vectors in Eq. (12) are chosen to satisfy the control objectives and these virtual components also provide as the reference inputs for the next step of the NSTASOSM design. These virtual controls can be expressed as Fig. 2. Ψ_{rd} rotor flux is identified in Section 3.3.

3.2. Designing NSTA_SOSM Controller for the Inner Current Loop Control

NSTA_SOSM controller for the inner current loop control in FOC vector control of SPIM drive. Stator current error is defined:

$$\begin{cases}\varepsilon_{isd} = i_{sd}^{*} - i_{sd} \\ \varepsilon_{isq} = i_{sq}^{*} - i_{sq}\end{cases} \tag{13}$$

The nonlinear improve slip surface according to the current components is chosen as follows:

$$\begin{bmatrix}s_1 \\ s_2\end{bmatrix} = \begin{bmatrix}\dfrac{d\varepsilon_{isd}}{dt} + \lambda_1.|\varepsilon_{isd}|^{1/2} sat(\varepsilon_{isd}) \\ \dfrac{d\varepsilon_{isq}}{dt} + \lambda_2.|\varepsilon_{isq}|^{1/2} sat(\varepsilon_{isq})\end{bmatrix} \tag{14}$$

Where $\lambda_1 > 0, \lambda_2 > 0$; We select the Lyapunov function:

$$V = \frac{1}{2}\left(\varepsilon_{isd}^2 + \varepsilon_{isq}^2\right) \tag{15}$$

Differentiate both sides of equation (16) we get:

$$\frac{dV}{dt} = \varepsilon_{isd}\frac{d\varepsilon_{isd}}{dt} + \varepsilon_{isq}\frac{d\varepsilon_{isq}}{dt} \tag{16}$$

To differentiate $V<0$, The current error differential function is chosen as follows:

$$\begin{cases}\dfrac{d\varepsilon_{isd}}{dt} = -k_{sd} v_{isd}(t) \\ \dfrac{d\varepsilon_{isq}}{dt} = -k_{sq} v_{isq}(t)\end{cases} \tag{17}$$

where: $k_1 = 1.5\sqrt{C_1}; k_2 = 1.1C_1; k_3 = 1.5\sqrt{C_2}; k_4 = 1.1C_2;$ with $C_1 > 0; C_2 > 0,$ From Eq. (4) (17), (18), (19) we get u_{sd} and u_{sdq} virtual control functions:

$$\begin{cases}u_{sd} = \dfrac{L_s}{c}\left[\dfrac{di_{sd}^{*}}{dt} + k_{sd} v_{isd}(t)\right] + \dfrac{1}{c}\left[a i_{sd} - L_s \omega_e i_{sq} - b R_r \psi_{rd}\right] \\ u_{sq} = \dfrac{L_s}{c}\left[\dfrac{di_{sq}^{*}}{dt} + k_{sq} v_{isq}(t)\right] + \dfrac{1}{c}\left[a i_{sq} - L_s \omega_e i_{sd} - b \omega_e \psi_{rd}\right]\end{cases} \tag{18}$$

3.3. Rotor Flux Identifier and Stability Analysis

The aim of this section is to estimate the rotor flux components based on the stator currents and voltages that are easily measurable as [41]. From current model (CM), the flux estimation algorithm based on sliding-mode theory is defined:

$$\begin{cases}\dot{\hat{\varphi}}_{rD} = \left(\dfrac{L_m}{T_r}\right) i_{sD} - \left(\dfrac{1}{T_r}\right)\hat{\varphi}_{rD} - \hat{\omega}_r \hat{\varphi}_{rQ} + \Lambda_{\varphi rD} I_s \\ \dot{\hat{\varphi}}_{rQ} = \left(\dfrac{L_m}{T_r}\right) i_{sQ} - \left(\dfrac{1}{T_r}\right)\hat{\varphi}_{rQ} + \hat{\omega}_r \hat{\varphi}_{rD} + \Lambda_{\varphi rQ} I_s\end{cases} \tag{19}$$

From (20), the dynamic of the estimation error is given by:

$$\begin{cases}\dot{\varepsilon}_1 = \left(\dfrac{K}{T_r}\right)\varepsilon_3 + K\omega_r \varepsilon_4 - \Lambda_{isD} I_s \\ \dot{\varepsilon}_2 = \left(\dfrac{K}{T_r}\right)\varepsilon_4 - K\omega_r \varepsilon_3 - \Lambda_{isQ} I_s \\ \dot{\varepsilon}_3 = \left(-\dfrac{1}{T_r}\right)\varepsilon_3 - \omega_r \varepsilon_4 - \Lambda_{\varphi rD} I_s \\ \dot{\varepsilon}_4 = \left(-\dfrac{1}{T_r}\right)\varepsilon_4 + \omega_r \varepsilon_3 - \Lambda_{\varphi rQ} I_s\end{cases} \tag{20}$$

By defining Lyapunov function as:

$$V = \frac{1}{2} S^T S \tag{21}$$

Whose time derivative is,

$$\frac{dV}{dt} = S^T \frac{dS}{dt} = \begin{bmatrix} \varepsilon_1 & \varepsilon_2 \end{bmatrix} \begin{bmatrix} \left(\frac{K}{T_r}\right)\varepsilon_3 + K\omega_r\varepsilon_4 - \Lambda_{isD} I_s \\ \left(\frac{K}{T_r}\right)\varepsilon_4 - K\omega_r\varepsilon_3 - \Lambda_{isQ} I_s \end{bmatrix} \tag{22}$$

when the currents trajectory reaches the sliding surface ε1=ε2=0, the observer error dynamics given by (39) behaves, in the sliding-mode as a reduced order system governed only by the roto flux error, because $\varepsilon_{is} = \dot{\varepsilon_{is}} = 0$. To demonstrate the stability of the previous system, the following Lyapunov function candidate is proposed:

$$V = \frac{1}{2}\begin{bmatrix} \varepsilon_3 & \varepsilon_4 \end{bmatrix}\begin{bmatrix} \varepsilon_3 & \varepsilon_4 \end{bmatrix}^T \tag{23}$$

The time derivative of the Lyapunov function candidate is:

$$\frac{dV}{dt} = \begin{bmatrix} \varepsilon_3 & \varepsilon_4 \end{bmatrix} \begin{bmatrix} \left(-\frac{1}{T_r}\right)\varepsilon_3 - \omega_r\varepsilon_4 - \Lambda_{\varphi rD} I_s \\ \left(-\frac{1}{T_r}\right)\varepsilon_4 + \omega_r\varepsilon_3 - \Lambda_{\varphi rQ} I_s \end{bmatrix} \tag{24}$$

When sliding takes place:

$$\begin{bmatrix} \Lambda_{\varphi rD} & 0 \\ 0 & \Lambda_{\varphi rQ} \end{bmatrix} = -\Lambda \begin{bmatrix} \frac{1}{T_r} & \omega_r \\ -\omega_r & \frac{1}{T_r} \end{bmatrix} \begin{bmatrix} \varepsilon_3 \\ \varepsilon_4 \end{bmatrix} = -\Lambda\Gamma \begin{bmatrix} \varepsilon_3 \\ \varepsilon_4 \end{bmatrix} \tag{25}$$

Choose $\Lambda = \Delta\Gamma^{-1}$ where $\Delta = \begin{bmatrix} \delta_1 & -\omega_r \\ \omega_r & \delta_2 \end{bmatrix}$ and δ_1, δ_2 are positive design constants. Note that det ($\Gamma(\omega_r)$)for all ω_r and so the inverse always exists.

$$\begin{bmatrix} \dot{\varepsilon}_3 \\ \dot{\varepsilon}_4 \end{bmatrix} = \left\{ \begin{bmatrix} -\frac{1}{T_r} & -\omega_r \\ \omega_r & -\frac{1}{T_r} \end{bmatrix} - \Delta\Gamma^{-1}\Gamma \right\} \begin{bmatrix} \varepsilon_3 \\ \varepsilon_4 \end{bmatrix} = \begin{bmatrix} \left(-\frac{1}{T_r}\right) - \delta_1 & 0 \\ 0 & \left(-\frac{1}{T_r}\right) - \delta_2 \end{bmatrix} \tag{26}$$

This is the flux observer error converges to zero with exponential rate of convergence.

4. Simulink and Discussion

The performance of the proposed BS_NSTA-SOSM controller for FOC vector control of SPIM drives is validated through simulation using MATLAB software. To increase the reliability, comparison frameworks are established, similar surveys are also implemented for the BS_INTSM, BS_SOSM [46] controller and compared with other latest methods in [14], [29], [30], [46], to confirm quantify the effectiveness of the proposed control structure. The analysis results also show the robustness and stability of the proposed controller in the face of parameter uncertainty and load disturbance, faster and more accurate dynamic response. The block diagram of the SPIM drive system

is shown in Fig. 3. 1HP, 6-phase, 220 *V*, 50 *Hz*, 4 poles, 1450 *rpm*. R_s = 10.1Ω, R_r = 9.8546Ω, L_s = 0.833457 *H*, L_r = 0.830811 *H*, L_m = 0.783106 *H*, *J* = 0.0088 $kg.m^2$.

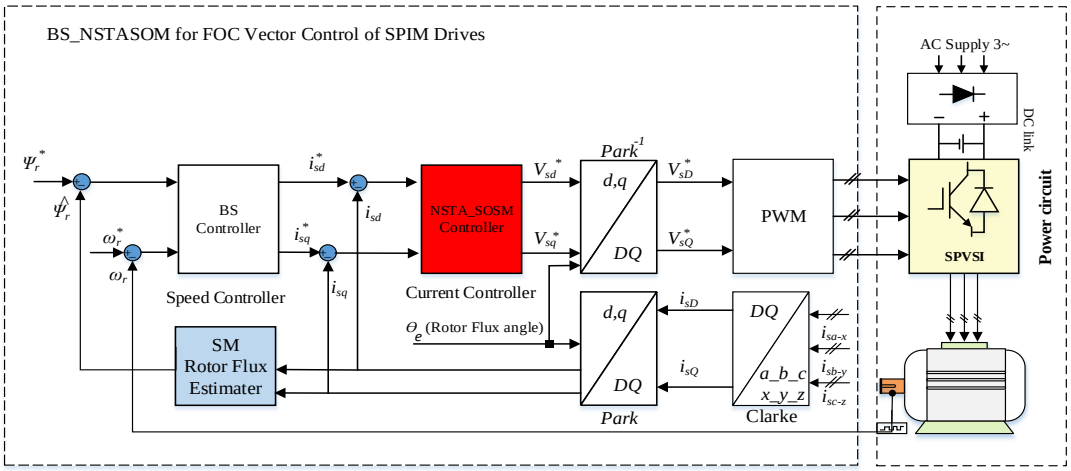

Fig. 3. Diagram of BS_NSTASOSM vector control for SPIM drives

4.1. Case 1

In this case, the SPIM drive works at high speed and the load torque changes. The survey is based on the experiments performed in [29], Fig. 7, Fig. 8, the speed is kept constant at 160 *rad/s* throughout the survey period, the load torque changes from 0 *Nm* - 7*Nm* at 0.8*s*.

Fig. 5 shows that, when the load disturbance is applied suddenly at *t* = 0.8s, there is an insignificant speed drop (decreases by 1.49 *rad/s*, ~ 0.9%) but immediately converges and works stably and accurately at the reference speed value (the speed error ~ 0), when the load disturbance is applied suddenly at *t* = 1.8*s*, the speed fluctuates around 0.1% and also immediately stabilizes, accurately tracking the set speed (speed error ~ 0).

On the contrary, when the load disturbance is closed, the speed decreases by 0.48 *rad/s*, but it cannot track exactly according to the reference. During the existence of load disturbances, speed errors are always different from 0. This process also happens in the same way when the load is rejected, the speed increases and the speed error does still not reach zero at the end of the survey. Observing the response of torque and flux, it is easy to see that there are fluctuations, the fluctuation ranges of torque are quite large when using the controller proposed in [29]. However, the phenomenon of torque and flux fluctuations does not appear when using the NSTA_SOSM controller. Torque and flux fluctuations are recorded quite large in [29] also shows that the main disadvantage of DTC compared to FOC is the Torque rip phenomenon as mentioned in the introduction and in [6]-[10], [29]. However, at the time of sudden load applying and speed changes, i_{sq} torque current response and electromagnetic torque response of SPIM using NSTA SOSM controller are higher overshoot compared to ISMC in [30]. Response of speed, torque, flux in case of variable load disturbance of controllers BS_INTSM and BS_NSTASOSM shown in Fig. 4.

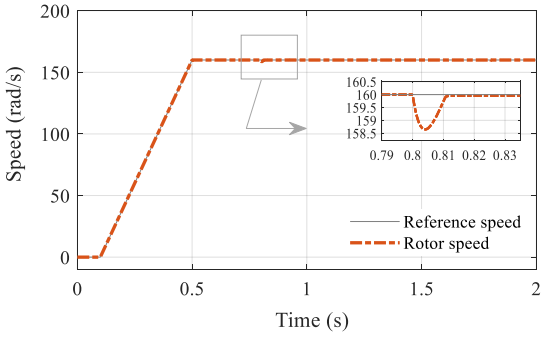

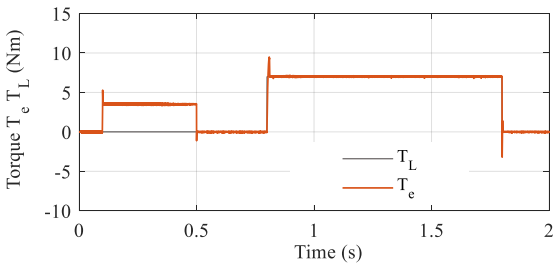

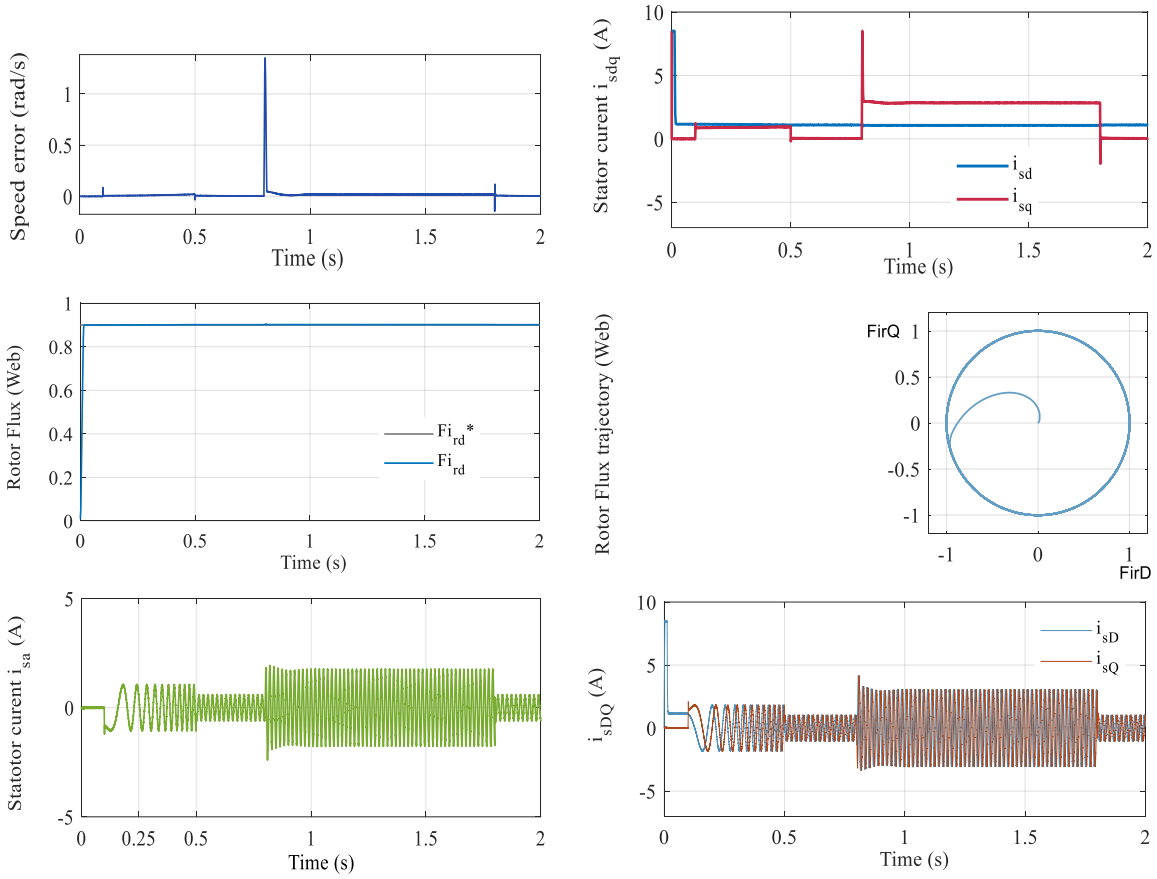

Fig. 4. Response of speed, torque, flux in case of variable load disturbance of controllers BS_INTSM and BS_NSTASOSM

Through this survey, it can be easy to see that NSTA SOSM controller provides fast, immediate and accurate response due to the use of STA in combination with SOSM and BS. The improved slip surface according to the current components is chosen (Eq. 15) allowing to eliminate effectively the chattering phenomenon. Besides, the design of controllers strictly complies with Lyapunov stability law helping the system work stably against sudden load changes. The advantages of SM's sustainability and immediate response are also clearly shown in this survey. However, the disadvantage of STA SOSM is the overshoot of the responses at the time appearing load disturband and speed change more higher than control method in [29]. This is considered an inevitable consequence when choosing a control solution that provides instantaneous responses of the NSTA SOSM controller, even though the overshoot time is very short (1/2 cycle) and immediately exact tracking the reference.

4.2. Case 2

In Fig. 6, a test is made to survey the reversing speed from -100rad/s to 100rad/s in a 2s cycle, repeating for 3 cycles the load disturbance is applied at t = 1.5 s. This survey is carried out based on the experiments in [30], Fig. 3 (3.1), which proposes the enhanced Integral Sliding Mode Control (ISMC), this survey is also carried out with the BS_INTSM, BS_SOSM [46] controller to get comparison data. On time the load torque is applied, the rotor speed drops but immediately tracks the desired speed properly, in steady state, the error is almost zero. The electromagnetic torque responds very quickly, smoothly, does not appear the torque ripple and chattering phenomena, isq torque current tracks the reference correctly. The rotor flux is kept stabling at the reference value.

Comparing with BS_SOSM in [46] and ISMC in [30], it can see that, the improvement of the second-order sliding surface, the proposed BS_NSTA SOSM controller generates isq torque current response and electromagnetic torque response at the time of sudden load applying and speed changes

has higher overshoot compared to ISMC in [30], but gives faster and more accurate, smoother response than BS_SOSM in [46] and ISMC in [30].

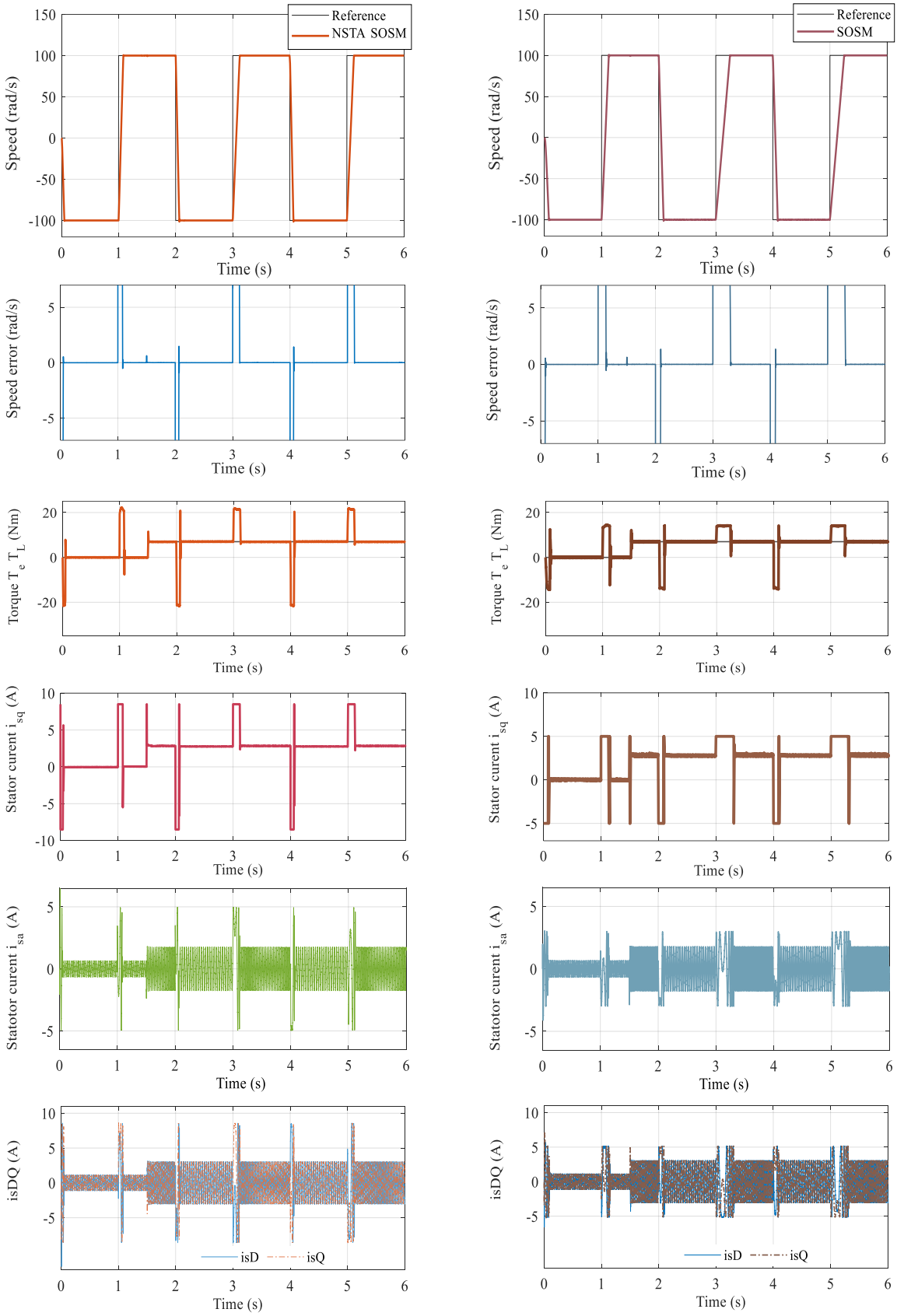

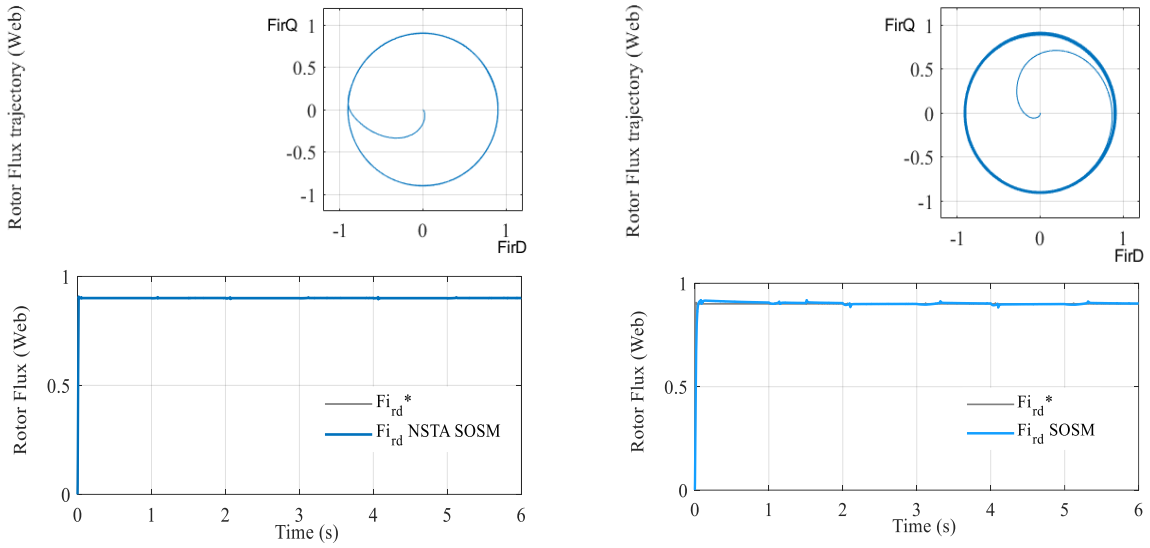

Fig. 5. Response of speed, torque, flux in case of variable load disturbance of controllers and (**a**) BS_NSTASOSM (**b**) BS_INTSM

4.3. Case 3

To more clearly verify the robustness of the BS_NSTA-SOSM controller against load disturbances and the impact of SPIM parameter changes, another survey was also performed under load disturbance conditions, machine parameters R_s, R_r varies in the low-speed range. This test is conducted based on the test proposed in [14] (Fig. 12, Fig. 13) but performed under harsher working conditions. In this test, the speed is kept constant at 25 rad/s, the external load step is varied from 0 to 100% of rated load at t=0.5s, R_s and R_r increase by 150% at t=1s (R_r*=2.5R_r, R_s* = 2.5R_s) (R_s*, R_r*: is the nominal stator and rotor resistance), at t=1.5 Rs and Rr decreases to 50% increase compared to the nominal value (R_r *=1.5R_r, R_s* = 1.5R_s).

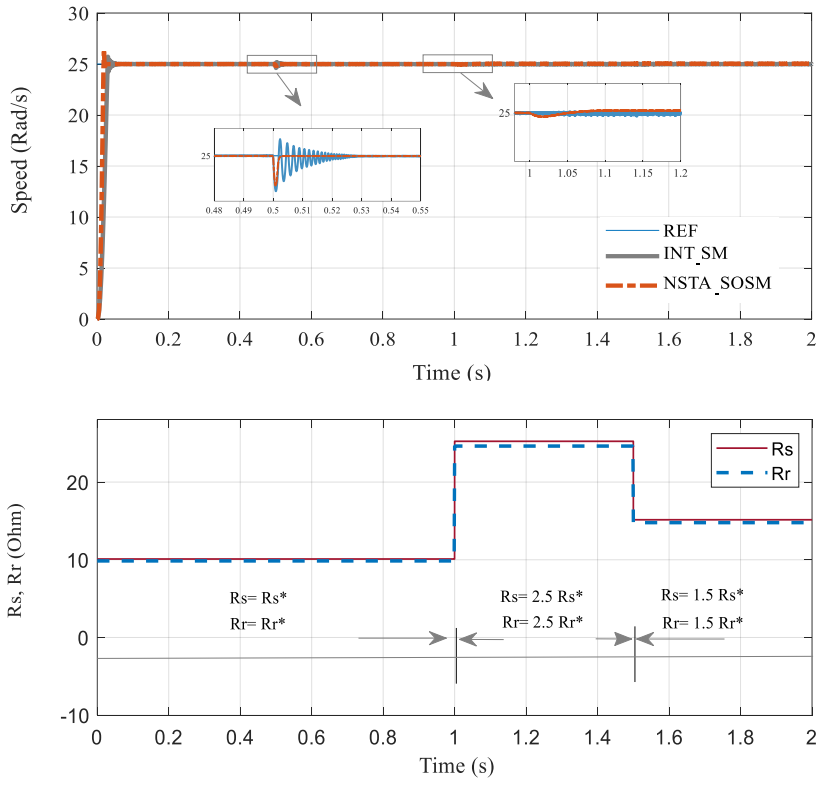

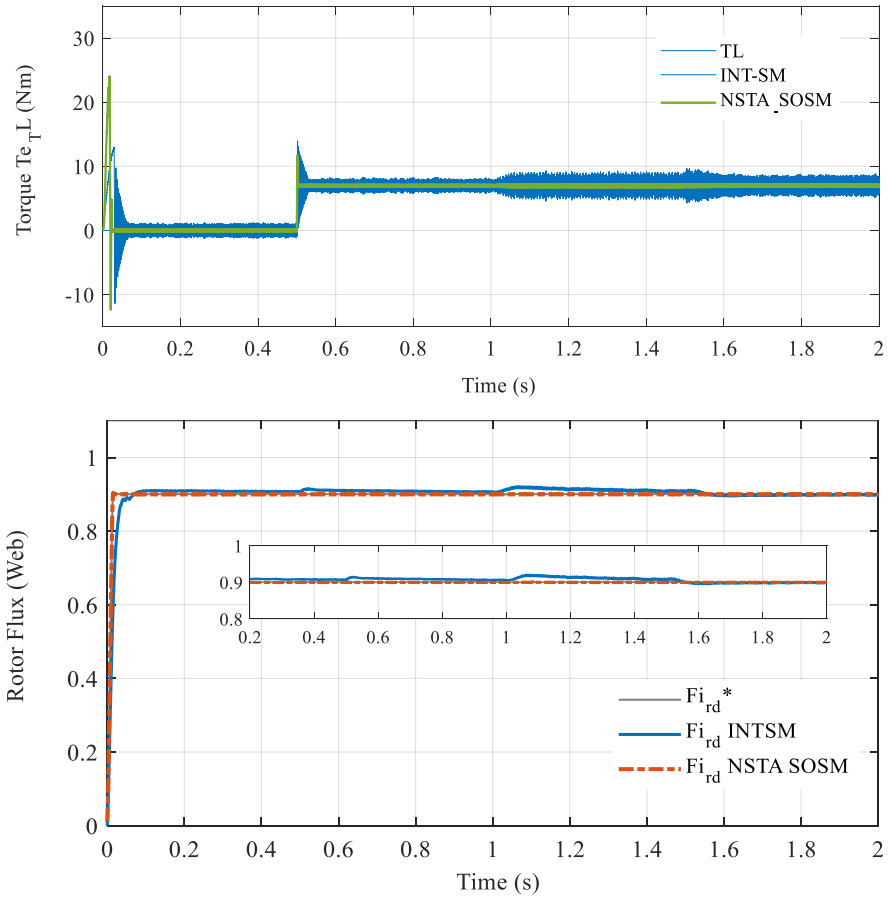

Fig. 6. Response of speed, torque, flux when parameters Rs, Rr change

Compare the results obtained in Fig. 6 and the results in [14], Fig. 12, Fig. 13, we see that the controllers can adapt when operating at low speeds, large load changes and uncertain parameters. However, the performance and robustness of the BS_NSTA-SOSM controller are the best in both transient and steady states as well as in the face of load disturbances and parameter variations. In Fig. 6, the BS_NSTASOSM speed is kept constant and exactly equal to the reference speed during most of the survey period, the oscillations of speed, torque and rotor flux are almost reported. On the contrary, with the BS_INTSM controller (Comparison of control strategies BS_INTSM and BS_NSTASOM, the results in Table 1 and Fig. 6, it is easy to see that the phenomenon of oscillation and chattering occurs during the entire survey period, chattering increases higher when Rs and Rr increase. These results also show that, despite being tested under more severe survey conditions, the BS_NSTA-SOSM controller shows better speed and torque response than PSO algorithm controller in [14], Fig. 12, Fig. 13, the torque and speed response [14] still oscillations.

The use of the improved slip surface in the NSTASOSM controller allows to eliminate effectively the chattering phenomenon. The controllers were designed strictly to comply Lyapunov stability law making the system work stably against the uncertain parameter and load disturbances. The advantages of SM's sustainability and immediate response are also clearly shown in this survey.

Table 1. Comparison of control strategies BS_INTSM and BS_NSTASOM with 100% rated load, $R^*_r = 2R_r$, $R^*_s = 2R_s$

	BS_INTSM	BS_NSTASOSM
Dynamics	Good	Excellent
Accurate tracking	Good	Excellent
Stability properties	Medium	Excellent
Robustness under Rr variations	Medium	Excellent
Chattering alleviation	Medium	Excellent

5. Conclusion

In this paper, the BS_NSTA_SOSM control structure for FOC vector control of SPIM drive is proposed. The simulation results have investigated under operating conditions at different speed ranges considering changes in machine parameters and external load disturbances show that the BS_NSTA-SOS controller works effectively on the one hand, it provides fast, accurate output responses, on the other hand, it enhances robust and stability of the SPIM drive and eliminates the chattering phenomenon. Similar surveys were also conducted for the BS_INTSM, BS_SOSM controller to establish a comparative framework, and analysis and comparison were also carried out with recently developed controllers in [14], [29], [30], [46]. These simulation results have demonstrated that the proposed controller has significantly improved the performance and robust of the SPIM drive, giving faster response speed, the steady-state error is approximately zero, and a smoother system. more robust and stable than the BS-INTSM, BS_SOSM controllers, and the controllers proposed in [14], [29], [30], [46]. However, besides the outstanding advantages mentioned above, the proposed BS_NSTA SOSM controller generates i_{sq} torque current response and electromagnetic torque response at the time of sudden load applying and speed changes has quite high overshoot, this is considered an inevitable consequence when choosing a control solution that provides instantaneous responses of the NSTA SOSM controller, even though the overshoot time is very short (1/2 cycle) and immediately exact tracking the reference. But this is also considered a weakness that needs to be seriously considered and overcome in the future. From the survey results obtained also shown that this is a promising strategy for the high-power industrial applications and the systems that require high quality control, reliability and capability high fault tolerance, Especially, in drive systems in electric vehicles, ships, In the future, the author to develop hardware to practically test this proposed control technique in the real system, the propulsion system of electric vehicle. First, perform small capacity tests in the laboratory and then test the electric vehicle model in practice.

Author Contribution: All authors contributed equally to the main contributor to this paper. All authors read and approved the final paper.

Funding: This research received no external funding.

Conflicts of Interest: The authors declare no conflict of interest

References

[1] A. Zemmit, S. Messalti, and A. Harrag, “A new improved DTC of doubly fed induction machine using GA-based PI controller,” *Ain Shams Engineering Journal*, vol. 9, no. 4, pp. 1877-1885, 2018, https://doi.org/10.1016/j.asej.2016.10.011.

[2] S. Boubzizi, H. Abid, and M. Chaabane, “Comparative study of three types of controllers for DFIG in wind energy conversion system,” *Protection and Control of Modern Power Systems*, vol. 3, no. 21, pp. 1-12, 2018, https://doi.org/10.1186/s41601-018-0096-y.

[3] M. Batool, A. Jalal and K. Kim, "Sensors Technologies for Human Activity Analysis Based on SVM Optimized by PSO Algorithm," *2019 International Conference on Applied and Engineering Mathematics (ICAEM)*, pp. 145-150, 2019, https://doi.org/10.1109/ICAEM.2019.8853770.

[4] M. Taoussi, M. Karim, D. Hammoumi, C. E. Bekkali, B. Bossoufi and N. E. Ouanjli, "Comparative study between backstepping adaptive and field-oriented control of the DFIG applied to wind turbines," *2017 International Conference on Advanced Technologies for Signal and Image Processing (ATSIP)*, pp. 1-6, 2017, https://doi.org/10.1109/ATSIP.2017.8075592.

[5] N. El Ouanjli, A. Derouich, A. El Ghzizal, A. Chebabhi and M. Taoussi, "A comparative study between FOC and DTC control of the Doubly Fed Induction Motor (DFIM)," *2017 International Conference on Electrical and Information Technologies (ICEIT)*, pp. 1-6, 2017, https://doi.org/10.1109/EITech.2017.8255302.

[6] I. Takahashi and T. Noguchi, "A New Quick-Response and High-Efficiency Control Strategy of an Induction Motor," *IEEE Transactions on Industry Applications*, vol. IA-22, no. 5, pp. 820-827, 1986, https://doi.org/10.1109/TIA.1986.4504799.

[7] T. Sutikno, N. R. N. Idris, and A. Jidin, "A review of direct torque control of induction motors for sustainable reliability and energy efficient drives," *Renewable and Sustainable Energy Reviews*, vol. 32, pp. 548-558, 2014, https://doi.org/10.1016/j.rser.2014.01.040.

[8] M. Dal, "Sensorless sliding mode direct torque control (DTC) of induction motor," *Proceedings of the IEEE International Symposium on Industrial Electronics, 2005. ISIE 2005*, vol. 3, pp. 911-916, 2005, https://doi.org/10.1109/ISIE.2005.1529045.

[9] N. E. Ouanjli, S. Motahhir, A. Derouich, A. E. Ghzizal, A. Chebabhi, and M. Taoussi, "Improved DTC strategy of doubly fed induction motor using fuzzy logic controller," *Energy Reports*, vol. 5, pp. 271-279, 2019, https://doi.org/10.1016/j.egyr.2019.02.001.

[10] X. Wu, W. Huang, X. Lin, W. Jiang, Y. Zhao and S. Zhu, "Direct Torque Control for Induction Motors Based on Minimum Voltage Vector Error," *IEEE Transactions on Industrial Electronics*, vol. 68, no. 5, pp. 3794-3804, 2021, https://doi.org/10.1109/TIE.2020.2987283.

[11] M. Yano, S. Abe, and E. Ohno, "History of power electronics for motor drives in Japan," *IEEE Conference on the History of Electronics*, 2004, https://ethw.org/w/images/4/49/Yano2.pdf.

[12] D. A. Dominic and T. R. Chelliah, "Analysis of field-oriented controlled induction motor drives under sensor faults and an overview of sensorless schemes," *ISA Transactions*, vol. 53, no. 5, pp. 1680-1694, 2014, https://doi.org/10.1016/j.isatra.2014.04.008.

[13] R. Kumar, S. Das, and A. Bhaumik, "Speed sensorless model predictive current control of doubly-fed induction machine drive using model reference adaptive system," *ISA Transactions*, vol. 86, pp. 215-226, 2019, https://doi.org/10.1016/j.isatra.2018.10.025.

[14] B. Kiyyour, L. Laggoun, A. Salhi, D. Naimi, G. Boukhalfa, "Improvement DTC for Induction Motor Drives Using Modern Speed Controllers Tuning by PSO Algorithm," *Periodica Polytechnica Electrical Engineering and Computer Science*, vol. 67, no. 3, pp. 249-259, 2023, https://doi.org/10.3311/PPee.21000.

[15] N. T. Pham and T. D. Le, "A Novel FOC Vector Control Structure Using RBF Tuning PI and SM for SPIM Drives," *International Journal of Intelligent Engineering and Systems*, vol. 14, no. 3, pp. 429-440, 2021, https://doi.org/10.22266/ijies2020.1031.38

[16] A. Bhaumik, S. Das, "Virtual voltage vector based predictive current control of speed sensorless induction motor drives," *ISA Transactions*, vol. 133, pp. 495-504, 2023, https://doi.org/10.1016/j.isatra.2022.07.007.

[17] N. T. Pham, T. D. Le, "A Novel Improved VGSTA BS_SM Control Structure for Vector Control of High Performance SPIM Drives," *International Journal of Intelligent Engineering and Systems*, vol. 15, no. 1, pp.155-166, 2022, https://doi.org/10.22266/ijies2022.0228.15.

[18] T. Wang, B. Wang, Y. Yu and D. Xu, "A Closed-Loop Voltage Model Observer for Sensorless Induction Motor Drives Based on the Orthogonality and Sliding-Mode Technique," *IEEE Transactions on Industrial Electronics*, pp. 1-15, 2024, https://doi.org/10.1109/TIE.2024.3374363.

[19] Y. Zhang *et al*., "Backstepping control of permanent magnet synchronous motors based on load adaptive fuzzy parameter online tuning," *Journal of Power Electronics*, 2024, https://doi.org/10.1007/s43236-024-00790-9.

[20] S. G. Jang, S. J. Yoo, "Predefined-time synchronized backstepping control of strict feedback nonlinear systems," *International Journal of Robust and Nonlinear Control*, vol. 33. no. 13, pp. 7563-7582, 2023, https://doi.org/10.1002/rnc.6765.

[21] D.Traoré, J. D. Leon, "Sensorless induction motor adaptive observer-backstepping controller: experimental robustness tests on low frequencies benchmark," *IET Control Theory*, vol 48, no. 11, pp. 1989-2002, 2010, https://doi.org/10.1049/iet-cta.2009.0648.

[22] R. Rinkeviciene, B. Mitkiene, "Design and Analysis Models with PID and PID Fuzzy Controllers for Six-Phase Drive," *World Electric Vehicle Journal*, vol. 15, no. 4, p. 164, 2024, https://doi.org/10.3390/wevj15040164.

[23] X. Liu, Y. Deng, J. Wang, H. Li and H. Cao, "Fixed-Time Generalized Active Disturbance Rejection with Quasi-Resonant Control for PMSM Speed Disturbances Suppression," *IEEE Transactions on Power Electronics*, vol. 39, no. 6, pp. 6903-6918, 2024, https://doi.org/10.1109/TPEL.2024.3377186.

[24] Y. Kali, J. Rodas, J. Doval-Gandoy, M. Ayala, O. Gonzalez, "Enhanced Reaching-Law-Based Discrete-Time Terminal Sliding Mode Current Control of a Six-Phase Induction Motor," *Machines*, vol. 11, no. 1, p. 107, 2023, https://doi.org/10.3390/machines11010107.

[25] D. Karboua, B. Toual, A. Kouzou, B. O. Douara, T. Mebkhouta, A. N. Bendenidina, "High-order Supper-twisting Based Terminal Sliding Mode Control Applied on Three Phases Permanent Synchronous Machine," *Periodica Polytechnica Electrical Engineering and Computer Science*, vol. 67, no. 1, pp. 40-50, 2023, https://doi.org/10.3311/PPee.21026.

[26] D. D. A. Souza, W. C. P. D. A. Filho and G. C. D. Sousa, "Adaptive Fuzzy Controller for Efficiency Optimization of Induction Motors," *IEEE Transactions on Industrial Electronics*, vol. 54, no. 4, pp. 2157-2164, 2007, https://doi.org/10.1109/TIE.2007.895138.

[27] A. Zaafouri, C. B. Regaya, H. B. Azza, A. Châari, "zDSP-based adaptive backstepping using the tracking errors for high-performance sensorless speed control of induction motor drive," *ISA Transactions*, vol. 60, pp. 333-347, 2016, https://doi.org/10.1016/j.isatra.2015.11.021.

[28] Y. Zahraoui, M. Akherraz, A. Ma'arif, "A Comparative Study of Nonlinear Control Schemes for Induction Motor Operation Improvement," *International Journal of Robotics and Control Systems*, vol. 2, no. 1, pp. 1-17, 2021, https://doi.org/10.31763/ijrcs.v2i1.521.

[29] Y. Zahraoui, M. Moutchou, S. Tayane, C. Fahassa, S. Elbadaoui, "Induction Motor Performance Improvement using Super Twisting SMC and Twelve Sector DTC," *International Journal of Robotics and Control Systems*, vol. 4, no. 1, pp. 50-68, 2024, https://doi.org/10.31763/ijrcs.v4i1.1090.

[30] F. Shiravani, P. Alkorta, J. A. Cortajarena, O. Barambones, "An Enhanced Sliding Mode Speed Control for Induction Motor Drives," *Actuators*, vol. 11, no. 1, p. 18, 2022, https://doi.org/10.3390/act11010018

[31] H. Maghfiroh, A. J. Titus, A. Sujono, F. Adriyanto, J. S. Saputro, "Induction Motor Torque Measurement using Prony Brake System and Close-loop Speed Control," *International Journal of Robotics and Control Systems*, vol. 2, no. 3, pp. 594-605, 2022, https://doi.org/10.31763/ijrcs.v2i3.782.

[32] I. Sami, S. Ullah, A. Basit, N. Ullah and J. Ro, "Integral Super Twisting Sliding Mode Based Sensorless Predictive Torque Control of Induction Motor," *IEEE Access*, vol. 8, pp. 186740-186755, 2020, https://doi.org/10.1109/ACCESS.2020.3028845.

[33] A. J. Abougarair, M. Aburakhis, M. Edardar, "Adaptive Neural Networks Based Robust Output Feedback Controllers for Nonlinear Systems," *International Journal of Robotics and Control Systems*, vol. 2, no. 1, pp. 37-56, 2022, https://doi.org/10.31763/ijrcs.v2i1.523.

[34] H. Maghfiroh, I. Iftadi, A. Sujono, "Speed Control of Induction Motor using LQG," *Journal of Robotics and Control*, vol. 2, no. 6, pp. 565-570, 2021, https://doi.org/10.18196/jrc.26138.

[35] D. Zellouma, H. Benbouhenni, Y. Bekakra, "Backstepping Control Based on a Third-order Sliding Mode Controller to Regulate the Torque and Flux of Asynchronous Motor Drive," *Periodica Polytechnica Electrical Engineering and Computer Science*, vol. 67, no. 1, pp. 10-20, 2023, https://doi.org/10.3311/PPee.20333.

[36] M. N. Huynh, H. N. Duong, V. H. Nguyen, "A Passivity-based Control Combined with Sliding Mode Control for a DC-DC Boost Power Converter," *Journal of Robotics and Control*, vol. 4, no. 6, pp. 780-790, 2023, https://doi.org/10.18196/jrc.v4i6.20071.

[37] J. E. Ruiz-Duarte and A. G. Loukianov, "Sliding mode output-feedback causal output tracking for a class of discrete-time nonlinear systems," *International Journal of Robust and nonlinear control*, vol. 29, no. 6, pp. 1956-1975, 2019, https://doi.org/10.1002/rnc.4470.

[38] I. O. Aksu and R. Coban, "Sliding mode PI control with backstepping approach for MIMO nonlinear cross-coupled tank systems," *International Journal of Robust and Nonlinear Control*, vol. 29, no. 6, pp. 1854-1871, 2019, https://doi.org/10.1002/rnc.4469.

[39] J. Qiu, W. Ji and M. Chadli, "A Novel Fuzzy Output Feedback Dynamic Sliding Mode Controller Design for Two-Dimensional Nonlinear Systems," *IEEE Transactions on Fuzzy Systems*, vol. 29, no. 10, pp. 2869-2877, 2021, https://doi.org/10.1109/TFUZZ.2020.3008271.

[40] N. T. Pham, T. D. Le, "A Sensorless Vector Control Using new BS_PCH Controller structure and SC MRAS Adaptive Speed Observer for Electric Vehicles," *WSEAS Transactions on Systems and Control*, vol. 15, pp. 366-374, 2020, https://doi.org/10.37394/23203.2020.15.38.

[41] N. T. Pham, K. H. Nguyen, "Sensorless Control for High Performance SPIM Drives Based on the Improved Rotor Flux Identifier Using Sliding Mode," *International Journal of Intelligent Engineering and Systems*, vol. 12, no.4, pp. 291-305, 2019, https://doi.org/10.22266/ijies2019.0831.27.

[42] N. T. Pham, "Sensorless speed control of SPIM using BS_PCH novel control structure and NNSM_SC MRAS speed observer," *Journal of Intelligent & Fuzzy Systems*, vol. 39, no. 3, pp. 2657-2677, 2020, https://doi.org/10.3233/JIFS-190540.

[43] C. Lascu, A. Argeseanu and F. Blaabjerg, "Supertwisting Sliding-Mode Direct Torque and Flux Control of Induction Machine Drives," *IEEE Transactions on Power Electronics*, vol. 35, no. 5, pp. 5057-5065, 2020, https://doi.org/10.1109/TPEL.2019.2944124.

[44] H. Li, W. Chou, "Adaptive FNN Backstepping Control for Nonlinear Bilateral Teleoperation with Asymmetric Time Delays and Uncertainties," *International Journal of Control, Automation and Systems*, vol. 21, pp. 3091-3104, 2023, https://doi.org/10.1007/s12555-022-0158-9.

[45] B. Farid, B. Tarek, B. Sebti, "Fuzzy super twisting algorithm dual direct torque control of doubly fed induction machine," *International Journal of Electrical and Computer Engineering*, vol. 11, no. 5, pp. 3782-3790, 2021, http://doi.org/10.11591/ijece.v11i5.pp3782-3790.

[46] N. T. Pham, "Speed Tracking of Field Oriented Control SPIM Drive using (BS_SOSM) Nonlinear Control Structure," *WSEAS Transactions on Systems and Control*, vol. 14, pp. 291-299, 2019, https://www.wseas.org/multimedia/journals/control/2019/a745103-871.pdf.

[47] W. Chen, S. S. Ge, J. Wu and M. Gong, "Globally Stable Adaptive Backstepping Neural Network Control for Uncertain Strict-Feedback Systems With Tracking Accuracy Known a Priori," *IEEE Transactions on Neural Networks and Learning Systems*, vol. 26, no. 9, pp. 1842-1854, 2015, https://doi.org/10.1109/TNNLS.2014.2357451.

[48] A. Pal, P. Roy and S. Ray, "Sliding Mode Speed Control of a Permanent Magnet Synchronous Motor using Twelve Sectors Modified DTC," *2022 IEEE Calcutta Conference (CALCON)*, pp. 128-132, 2022, https://doi.org/10.1109/CALCON56258.2022.10060752.

[49] N. T. Pham, "Discrete-time Sensorless Control Using new BS_SM Controller structure and VM_ SC MRAS Adaptive Speed Observer for The propulsion system of Ship," *WSEAS Transactions on Systems and Control*, vol. 19, pp. 257-267, 2020, https://doi.org/10.37394/23201.2020.19.28.

[50] N. Derbel, J. Ghommam, Q. Zhu, "Applications of Sliding Mode Control," *Springer*, vol. 79, 2017, https://doi.org/10.1007/978-981-10-2374-3.